Ammonia emissions from a grazed field estimated by miniDOAS measurements and inverse dispersion modelling

Michael Bell[1], Christophe Flechard[1], Yannick Fauvel[1], Christoph Häni[2], Jörg Sintermann[3a],
Markus Jocher[3], Harald Menzi[4], Arjan Hensen[5], Albrecht Neftel[3b]

[1]INRA, Agrocampus Ouest, UMR 1069 SAS, Rennes, France
[2]Bern University of Applied Sciences, School of Agricultural, Forest and Food Sciences, CH-3052 Zollikofen,
Switzerland
[3]Agroscope - Institute for Sustainability Science, Zürich, Switzerland
[4]Federal Research Station Agroscope, Inst. For Livestock Sciences, 1725 Posieux, Switzerland
[5]Energy research Centre of the Netherlands (ECN), Petten, The Netherlands
[a]now at AWEL, Zürich, Switzerland
[b]now at Neftel research Expertise, C -3033 Wohlen b. Bern, Switzerland

Correspondence to: Michael Bell (michael.bell@inra.fr)

Abstract

Ammonia (NH_3) fluxes were estimated from a field being grazed by dairy cattle during spring, by applying a backward-Lagrangian Stochastic model (bLS) model combined with horizontal concentration gradients measured across the field. Continuous concentration measurements at field boundaries were made by open-path miniDOAS (differential optical absorption spectroscopy) instruments, during the cattle's presence and for 6 subsequent days. The deposition of emitted NH_3 to 'clean' patches on the field was also simulated, allowing both 'net' and 'gross' emission estimates, where the dry deposition velocity (v_d) was predicted by a canopy resistance (R_c) model developed from local NH_3 flux and meteorological measurements. Estimated emissions peaked during grazing and decreased after the cattle had left the field, while control on emissions was observed from covariance with temperature, wind speed and humidity/wetness measurements made on the field, revealing a diurnal emission profile. Large concentration differences were observed between downwind receptors, due to spatially heterogeneous emission patterns. This was caused by uneven cattle distribution and a low grazing density, where 'hotspots' of emissions would arise as the cattle grouped in certain areas, such as around the water trough. The spatial complexity was accounted for by separating the model source area into sub-sections, and optimising individual source area coefficients to measured concentrations. The background concentration was the greatest source of uncertainty, and based on a sensitivity/uncertainty analysis the overall uncertainty associated with derived emission factors from this study is at least 30-40%.

Emission factors can be expressed as 6 ± 2 g NH_3 cow^{-1} day^{-1}, or $9 \pm 3\%$ of excreted urine-N emitted as NH_3, when deposition is not simulated, and 7 ± 2 g NH_3 cow^{-1} day^{-1}, or $10 \pm 3\%$ excreted urine-N emitted as NH_3 when deposition is included in the gross emission model. The results suggest that around $14 \pm 4\%$ of emitted NH_3 was deposited to patches within the field that were not affected by urine or dung.

1. Introduction

Over 90% of anthropogenic ammonia (NH_3) emissions in Europe have agricultural sources (Erisman et al., 2008; Reidy et al., 2008; Hertel et al., 2011), 70-90% of which have been estimated to be produced by livestock (Pain et al., 1998; Hutchings et al., 2001). In addition to decreasing nitrogen efficiency for farming systems, the volatilisation of NH_3 from agricultural areas is a principal factor in the formation of fine fraction secondary aerosols due to its reactions with nitric and sulphuric acids in the atmosphere, and upon deposition is linked to acidification and eutrophication of natural ecosystems (Sutton et al., 2011). Following the application of urine and dung to the soil surface by grazing livestock, urea is microbially converted to NH_3 which is volatilised at rates which vary extensively depending on soil and canopy layer properties, weather, and culture conditions (Laubach et al., 2013a). It has been estimated that 75-90% of the N ingested by a grazing cow is metabolised inefficiently and returned by excreta to the grazing paddocks, of which over 70% is returned as urine (Whitehead, 1995; Zaman et al., 2009). NH_3 emissions have been measured from cattle urine patches at the ratio of 7-25.7% of excreted urine nitrogen (N) for grazed pastures (Jarvis et al., 1989; Ryden et al., 1987; Laubach et al., 2012; 2013a), and measurements from sheep urine patches in summer-winter experiments have suggested emissions which represent 12.2–22.2% of excreted urine-N (Sherlock and Goh, 1984).

Methods for estimating emissions from grazed pastures include micrometeorological methods, where profiles of concentration and wind speed are measured at one or more points downwind from the source, allowing fluxes to

54   be calculated using the theory of turbulent transport in the atmospheric surface layer (Laubach et al., 2012).

55   Dynamic chambers or movable wind tunnels may be used to estimate emissions from simulated grazing in the

56   laboratory or the field (Sommer et al., 2001). However enclosure measurements may not always be

57   representative of emissions at the field scale (Genermont and Cellier, 1997; Sintermann et al., 2012). The

58   inverse dispersion method concerns the inferring of the atmospheric emission rate (Q) of localised gas sources

59   from the excess concentration (ΔC) they cause above background, by modelling the $\Delta C / Q$ relationship for a

60   given measurement setup under the existing meteorological state (Flesch et al., 2004; Flesch et al., 2014).

61   The local dry deposition of NH_3 within the grazed field is an important consideration to make, as in contrast to

62   other pollutants a significant proportion may be deposited locally (e.g. Loubet et al., 2009). The proportion of

63   deposited NH_3 is sensitive to multiple parameters, including the source height, wind speed, atmospheric

64   stability, land cover type and the numerous specific surface parameters therein (e.g. Sutton et al. 1993). This

65   leads to modelling results that vary widely, with local recapture ranging from 2% to 60% within 2km from the

66   source (Loubet et al., 2006, Asman et al., 1998). Accordingly, the modelling of NH_3 deposition can be a

67   challenging undertaking, with models ranging from simple steady-state canopy resistance models to dynamic,

68   bi-directional, multi-layer and multi-process chemical species schemes (Flechard et al., 2013). Local-scale

69   deposition models may ignore the wet deposition process, as dry deposition is most likely the dominant dry

70   deposition mechanism near sources (Loubet et al., 2009).

71   In this study, a bLS dispersion model with a coupled dry deposition scheme has been applied to estimate the

72   NH_3 emissions from a field being grazed by dairy cows, using the horizontal concentration gradients measured

73   across the field by three open-path miniDOAS instruments (Sintermann et al., 2016; Volten et al., 2012). The

74   open-path measurement system is to considerable benefit, as most techniques to measure atmospheric NH_3 are

75   sampling techniques and therefore involve inlet contact with the highly adhesive NH_3, which may slow response

76   times and lead to interaction with water molecules and interference by ammonium aerosols dissociating on tubes

77   or filters (e.g. von Bobrutzki et al., 2010). The miniDOAS system is a comparatively interference-free

78   measurement technique, since it utilises the wavelength-dependent UV-light absorption of NH_3 over an open

79   light path. The system also has capacity for long-term fast response continuous measurements, and a broad

80   measurement path which makes the miniDOAS well-suited concentration receptors for monitoring the

81   fluctuations in NH_3 concentrations across field boundaries.

82   The objectives of our study were: (1) to evaluate the NH_3 emissions from cattle grazing using the bLS

83   dispersion technique and contribute towards an emission factor, as there is a limited number of existing

84   measurements, (2) to simulate the degree of re-deposition that occurs within the field, and (3) evaluate the

85   application of the bLS technique and the miniDOAS measurement system to derive NH_3 fluxes from

86   agricultural diffuse sources such as grazing. The bLS model assumes a homogenous source area, therefore it

87   was assumed that emission estimates would be insensitive to irregular cattle distribution and excretion patterns.

88   The measurement of concentration gradients across grazed fields is challenging, as downwind concentration

89   levels may not rise far above background as is the case with stronger sources, such as applied slurry. Therefore

90   this is an exercise which requires precise and continuous measurements from two or more sensors to evaluate

91   (ΔC). However the method is also nonintrusive and is not labour intensive, and can provide continuous emission

92   estimates over long or short time periods if the conditions and experimental design are in agreement.

2. Methods

2.1 Site description and experimental design

The experiments were conducted from 18-29 May 2015, on a rectangular grazing pasture of about two hectares at the INRA-Méjusseaume dairy research experimental farm in NW France (48.11704, -1.79736). The site was flat and benefited from a lack of wind-disturbing elements within 100m of the field boundaries (e.g. trees, buildings or other protruding elements). The cattle were not given additional feed to supplement grazing (mixed grass sward rich in *Lolium perenne*). The field had been previously grazed one month prior (16-27 May 2015) to the beginning of the experiment, and mineral fertiliser had been applied on 31/03. During measurement Period 1, 25 cows were allowed to graze within the southwestern section of the field (Area D, Figure 1) from 08:00 18/05 - 15:00 20/05 UTC (28 hours grazing), with three sets of miniDOAS open-path sensors and placed along the northern, western and eastern boundaries. The miniDOAS sensors were placed to optimise the measurement of (ΔC) across the field after reviewing wind directions forecast for the week ahead. The miniDOAS sensors have been given the names S1, S2 and S3, where the S2 sensor was placed upwind of the grazed field while the S1 and S3 sensors were placed at downwind locations. During Period 2, the whole field (Areas A, B, C, D) was opened for 44 grazing cattle, with the cattle present on the field from 10:00 20/05 – 05:00 23/05 (60 hours grazing), while the miniDOAS sensors were left in place to measure residual emissions from 23-29/05. The cattle were removed from the field for milking during both periods for roughly one hour twice per day. As the field area during Period 2 was much larger, the S2 and S3 miniDOAS sensors were moved to the north-western and south-eastern field boundaries respectively, leaving the three miniDOAS paths in-line with a NW-SE transect of the field (Figure 1). The grazing densities during Periods 1 and 2 were 44 and 22 cattle ha^{-1}, respectively.

2.2 Ammonia measurements

The DOAS technique is based upon the wavelength dependent absorption of light over a specified light path. The miniDOAS instruments offer greater portability and a lower cost relative to prior DOAS instruments (Volten et al., 2012). The broadband and narrowband extinction of UV-light (=absorption + scattering) is measured across the light path, and the concentration of different trace gases is determined by their respective absorption spectra (details in Sintermann et al., 2016). In the wavelength range used by the miniDOAS (204 – 230nm), narrowband-absorption is seen by NH_3, sulphur dioxide (SO_2), and nitrogen oxide (NO), while other absorbers with broader absorption features are eliminated by high-pass-filtering. The systems were calibrated using a flow-cell in the miniDOAS light path with a high-concentration NH_3 gas standard; in addition the cell's outlet-flow was checked by wet chemical impinger samples (two in a row) and photometric NH_3 determination. Details are presented by Sintermann et al., (2016). Reference spectra (I_{ref}, see Sintermann et al., 2016) were determined for each instrument during an inter-comparison phase at the field site one week prior to the grazing experiment, where the three miniDOAS systems were configured to measure in parallel (measuring concentrations across the same open-path). In order to provide the absolute concentration reference (c_{ref}, see Sintermann et al., 2016) for the miniDOAS, a transect of three sets of ALPHA passive sampler triplicates (Tang et al., 2001) were placed along the path length, giving a time-integrated c_{ref} measurement. The miniDOAS inter-comparison showed close agreement in the concentration levels between the three systems, where the coefficient

131 of variation was 3.4% (unpublished data). A revision of the calibration procedure applied by Sintermann et al.

132 (2016) led to an increase in the slope by 16%, due to a gas standard correction in the conversion from ppm to µg

133 m^{-3}.

134 To measure horizontal concentration gradients across the field, three miniDOAS instruments were placed

135 strategically (based on the forecasted wind direction) at field boundaries at heights 1.4m above the ground, on

136 stands drilled into the ground for stability. Retro-reflectors were set 37m away from each light source at the

137 same height. A sensor placed upwind of the field would measure the background concentration (C_b), which can

138 be subtracted from the downwind concentration measurements (C) to determine the horizontal concentration

139 gradient or excess in concentration caused by emissions (ΔC). The miniDOAS concentration measurements

140 were recorded at 1-minute averaging intervals, and later averaged to 30 minute intervals for analysis.

2.3 Micrometeorological measurements

142 A three-dimensional ultrasonic anemometer (Gill Windmaster, Gill Instruments Limited, Lymington, UK) was

143 mounted on an instrument tower at 1.5m height above the ground within a fenced-off section in the centre of the

144 field. The three orthogonal wind components (u, v, w, m s^{-1}) and a temperature measurement were logged at a

145 frequency of 20 Hz. Later the eddy covariance measurements were processed over 30 minute averages, and the

146 friction velocity ($u*$, m s^{-1}), surface roughness (z_0, cm), Monin-Obukhov length (L, m), standard deviations of

147 the rotated wind components ($\sigma_u, \sigma_v, \sigma_w$), and resultant horizontal wind speed (u, m s^{-1}) and wind direction

148 (wd) were computed. Correction factors were applied to fix a 'bug' implicit within the Gill Windmaster

149 instrument, as recommended by the manufacturer (Gill Instruments, 2016). The applied correction was a

150 multiplication factor of 1.166 applied to positive vertical w wind axis measurements, and a factor of 1.289

151 applied to negative w wind axis measurements.

152 Mounted on the instrument tower at 2m height was a HMP45C sensor (Campbell Scientific, Loughborough,

153 UK) which provided temperature (T, ℃) and relative humidity (RH, %) measurements. Leaf wetness (LW, %

154 time wet) at canopy level was measured by a specialised conductivity sensor (Campbell Scientific,

155 Loughborough, UK) placed 10 cm above the ground.

2.4 Dispersion modelling

157 The backward Lagrangian Stochastic (bLS) type dispersion model is frequently applied for the computation of

158 the inverse dispersion method (Flesch et al., 2004). Driven by measurements of the prevailing wind conditions,

159 and with knowledge of the rise in concentration above background (ΔC) caused by an emitting source, the

160 model can be applied to estimate the emission rate that best fits the measured concentration data. During bLS

161 simulation the trajectories of thousands of fluid particles are calculated backwards in time from a reference point

162 (concentration receptor) under the prevailing wind conditions. The locations where the trajectories intersect the

163 ground ("touchdowns") and proportion of these which fall within the source area (N_{source}) are used to calculate

164 ($\Delta C/Q$), along with the associated vertical velocity (w_0) of each touchdown (Flesch et al., 2005).

165 The bLS-R model (Häni, 2016), is an inverse dispersion model that is based upon the backward Lagrangian

166 stochastic dispersion theory described by Flesch et al., (1995; 2004); however bLS-R has an additional function

167 which computes the effect of dry deposition on gas concentrations. The bLS-R package provides functions to set

168 up and execute the model within the R statistical software (R Core Team, 2015). The model calculates the

169   dispersion coefficient D (s m^{-1}), used to derive the flux emitted from the source (Q, μg m^{-2} s^{-1}), by the measured

170   rise in concentration above background (ΔC) (Eq. 1).

171
$$Q = (\Delta C) * D^{-1} \qquad (1)$$

172   where D is retrieved by the model from the number of source area interactions (N_{source}) and the thousands of

173   trajectories (N) released backwards in time from the receptor locations (Eq. 2).

174
$$D = \frac{1}{N}\sum N_{source} \left|\frac{2}{w_0}\right| \qquad (2)$$

175   The following input data were applied in the bLS-R model as 30 minute averages: wind direction, friction

176   velocity ($u*$) the standard deviations of the rotated wind vector components ($\sigma_u, \sigma_v, \sigma_w$), and surface roughness

177   (z_o). The spatial dimensions of the grazed field source area and the miniDOAS receptors were also specified.

178   Independent concentration measurements and emission estimates were derived using the two downwind

179   miniDOAS receptors (S1 and S3), which are compared throughout the paper, e.g. $CS1$, $CS3$ and $QS1$, $QS3$. All

180   concentrations and fluxes are expressed in units of NH$_3$, e.g. μg NH$_3$ m^{-3} and μg NH$_3$ m^{-2} s^{-1}.

181   **2.5 Data filtering**

182   The miniDOAS NH$_3$ measurements were filtered to remove periods of high uncertainty, indicated by the

183   standard error (SE) of the measurements. This filter only affected the S1 miniDOAS sensor, which was not

184   fitted with an automatic alignment system to correct minor shifts in the light path between lamp and reflector.

185   After applying this filter 92 out of 430 half hourly measurements were removed from the Period 2 S1

186   measurements (Period 1 measurements were unaffected).

187   Previous studies (Flesch et al., 2004; Harper et al., 2011) have applied $u*$ and Monin-Obukhov length (L)

188   filtering to remove emission estimates that do not meet given criteria ($u* > 0.15$ ms^{-1} and $L > 10$m). These

189   criteria were established on the basis of an observed reduction in the accuracy of model predictions as $u*$ and L

190   decrease (e.g., Flesch et al., 2004; Gao et al., 2009). However filtering out periods with low wind speeds and

191   unstable stratification can be detrimental to emission estimates, often creating a bias to characterise certain

192   sources under specific daytime or night-time conditions, whilst ignoring potentially valuable data that do not

193   meet the criteria. This is a major limitation as we calculate average emissions from grazing cattle, where strong

194   diurnal cycling is expected to occur (e.g. Laubach et al., 2013a). Flesch et al., (2014) developed alternate criteria

195   for bLS data filtering, finding that (for their particular experiment) the $u*$ threshold could be reduced to 0.05 m

196   s^{-1}, and after finding no improvement after imposing a stability (L) filter, introduced a supplementary vertical

197   temperature gradient filter.

198   A filtering procedure was developed after assessing the standard error (SE) of emission estimates ($\sigma_{Q/Q}$), which

199   describes period-to-period fidelity and identifies "spiking" in model predictions caused by unsuitable input

200   conditions, which do not confirm to an underlying assumption of a horizontally homogenous surface layer

201   (Flesch et al., 2014). It was found that a $u*$ threshold of 0.1 m s^{-1} was sufficient to remove the significant

202   outliers, while retaining acceptable data coverage, although this filter was at times limiting for nocturnal (low

203   wind) periods. A wind direction filter was applied to remove periods where miniDOAS sensors S1 and S3 were

204   not downwind of the field area. This filter only affected sensor S3 during Period 2, where estimates were

205   ignored if $wd > 30$ & $wd < 270$.

206   **2.6 Modelling of dry deposition within the source area**

207   Downwind from a source of NH_3, local recapture will remove a certain fraction of emitted NH_3 from the air.

208   Therefore the measured rise in concentration above background (ΔC) is a function of the source emission rate,

209   atmospheric dispersion, and the fraction that has been deposited. Within a field being grazed by dairy cattle,

210   emissions of NH_3 are expected from urine and dung patches, while deposition will occur to clean surfaces

211   within and beyond the field. Therefore, as we apply the bLS method to estimate emissions from the measure

212   concentration gradient across the field (ΔC), we calculate the "net" flux constituting emissions from the field

213   minus the fraction that has been deposited. However, if dry deposition is simulated in the dispersion model the

214   lost fraction of emissions due to deposition can be quantified, providing an estimate for the "gross" emissions

215   from excretions during grazing.

216   The bLS-R model has a post-processing routine to take into account the effect of the dry deposition of NH_3 on

217   flux predictions. The exchange or deposition velocity (v_d) is based upon a uni-directional resistance model

218   approach, defined as the inverse of a sum of a series of resistances to deposition (Eq. 3, left side).

219
$$v_d = \frac{1}{R_a + R_b + R_c} = \frac{-F}{C} \qquad (3)$$

220   where R_a is the aerodynamic resistance to transfer through the turbulent surface layer for a certain reference

221   height, R_b is the boundary layer resistance associated with the viscous quasi-laminar sublayer adjacent to the

222   deposited surface, and R_c is the canopy resistance representing the combined surface resistance accounting for

223   stomatal and non-stomatal pathways to deposition (Flechard et al. 2013). It should be noted that R_a is implicit

224   within the bLS-R calculations and does not need to be input to the model as a variable.

225   The resistances to deposition R_a and R_b can be calculated using ultrasonic anemometer measurements and well-

226   established models (Asman, 1998), while R_c is a composite term representing numerous physical barriers to

227   deposition at the surface. To obtain local, field-scale estimates of R_c, Two COTAG systems (conditional time-

228   averaged gradient systems, Famulari et al., 2010) were operated at the centre of the grazed field for 1.5 years,

229   allowing R_c to be estimated from calculations of R_a and R_b and time-integrated measurements of NH_3

230   concentration (C), flux ($-F$) and v_d (Eq. 3). The COTAG measurements were filtered to remove grazing

231   periods and periods up to two weeks after grazing had ended, to ensure 'clean' background conditions. Clear

232   correlation was then observed between the time-integrated R_c estimates with the variables T and RH, thus a

233   double exponential equation was parameterised as follows to fit the data (Eq. 4, Figure 2), with similar form to

234   Flechard et al., (2010):

235
$$R_c = R_{c,\,min} \times exp^{\alpha \times (100-RH)} \times exp^{\beta \times Abs(T)} \qquad (4)$$

236   A curve fitting procedure provided estimates of the parameters α, β and $R_{c,\,min}$ as 0.013 and 0.015 and 10 s m^{-1},

237   respectively.

238   The deposition component of bLS-R operates on the assumption that the whole grazed field is acting as a

239   homogenous surface for deposition, however in reality urine and dung patches on the field are obviously

240   hotspots of emissions, and not NH_3 sinks. The ratio of 'clean canopy' where deposition may occur to 'soiled

241   canopy' is not known, thus it is difficult to provide a true emission estimate including the effect of deposition.

242   We can expect that the emission estimate without deposition (Q) represents a 'net' emission rate from the field,

243   while if we assume that the whole field behaves as homogenous sink, the emission rate including deposition will

244   represent an upper limit of the gross emission estimate. The actual emission rate for a soiled field can be

245   expected to fall somewhere in between the net and upper gross estimates.

246   A means of addressing this issue with the heterogeneous canopy surface may be found in reviewing the R_c

247   timeseries derived from the time-integrated COTAG concentration and flux measurements on the field, as v_d

248   acts on the local vertical concentration gradient between surface and reference height, i.e. the flux is

249   concentration-gradient driven. At certain periods over the course of the year cattle were brought onto the field

250   for grazing, and shortly after the grazing periods had ended the NH_3 flux would return back to the negative

251   (deposition), and therefore R_c could be calculated. Averaging all of the COTAG R_c calculations within one

252   month following each grazing period gives an R_c value of 260 s m^{-1}, and comparing this value with the average

253   R_c where there had been no grazing on the field for at least one month (130 s m^{-1}). Therefore fertilisation of the

254   field surface through grazing appears to have caused an increase in R_c of 130 s m^{-1}. This measured increase

255   caused by excreted N to the field surface has been applied as an offset to the modelled R_c estimated by Eq. 4,

256   and has been input to bLS-R. The bLS emission estimates without including deposition are referred to as Q,

257   while the estimates including deposition and the R_c offset are referred to as Q_{dep}. Emission estimates including

258   deposition but without the R_c offset are referred to as Q_{depmax}.

259   **2.7 N excretion model**

260   To contribute towards an emission factor for cattle grazing and to compare with literature values, it was

261   necessary to express the emission estimates as a fraction of excreted N or urine-N. A nitrogen excretion model

262   based on the Swiss feeding recommendations for dairy cows (Menzi et al. 2015; Muenger personal

263   communication) was applied to quantify the total N and urine-N excreted to the field during both grazing

264   periods, from the following set of inputs: (1) milk yield, (2) animal numbers, average weight and date after

265   calving, (3) the net energy for lactation (NEL) and crude protein (CP) content of the grass, (4) the number of

266   animals grazed and the duration of grazing on the experimental plot. The excretions per day were calculated as

267   consumption minus retention in milk and animal growth. The share of N excreted in faeces and urine was

268   calculated using regressions of fecal N digestibility derived from N balance studies (Bracher et al. 2011, 2012).

269   **3. Results**

270   **3.1 Period 1 (18-20/05): grazing on SW paddock only**

271   **3.1.1 Concentration measurements**

272   The wind direction during Period 1 was consistently W-WSW (Figure 3). Therefore DOAS S2 was located

273   upwind of the grazed SW paddock while S1 and S3 were situated downwind to the eastern and northeastern

274   boundaries of the field respectively. Concentrations across the S2 path length would be expected to be low and

275   near background, except during periods of very low wind speed, while any rise in concentration measured by S1

276   and S3 above S2 would show the influence of emissions from the field.

277   The upwind S2 concentration measurements reveal background concentrations of 2-3 μg m^{-3} during times of

278   steady W/SW winds, increasing slightly when wind speed was low. Concentration polar plots (Figure 3) show

279   the average concentrations measured as a function of wind speed and direction, where the influence of emissions

280 from the grazed field is illustrated by the increase in measured concentrations at downwind receptors S1 and S3

281 relative to S2 (C_b).

282 Power failure led to a partial loss of measurements from miniDOAS S2, which are required to specify C_b for

283 estimating emissions through bLS modelling. A significant linear regression was found between the measured

284 background S2 concentration and wind speed (u), temperature (T) and relative humidity (RH):

285 $$C_b\ =\ 4.26 - 0.59u\ +\ 0.06T - 0.017RH,\ \mathrm{r}^2 = 0.5 \tag{5}$$

286 The wind direction remained consistent after the S2 power failed on 19/05, therefore the empirical relationship

287 (Eq. 5) was found to be suitable and was applied to estimate and extend S2 concentrations, as a proxy for C_b.

288 The predicted S2 concentrations follow the measured S2 concentrations closely until the point of data loss on

289 19/05 (Figure 4, top panel). This lends confidence to the rest of the C_b predictions used to fill the gap in the

290 measurements, even though there is increased uncertainty associated with the last 15 hours of emission

291 estimates calculated from the predicted C_b, relative to periods where C_b was measured by the S2 sensor.

3.1.2 Field-scale emissions estimates

293 Overall there is very good agreement between the emission calculations from both downwind concentration

294 datasets. The average emission rate calculated by bLS-R for the S3 measurements (QS3) is 0.29 µg m^{-2} s^{-1},

295 while the QS1 average is 0.27 µg m^{-2} s^{-1}. The modelled emission of NH$_3$ is low (generally below 0.2 µg m^{-2} s^{-1})

296 during the first 24 hours, as the measured concentration gradient across the field was less than 1 µg m^{-3}. As the

297 cattle were introduced to the field on the first morning (18/05) it likely took some time for NH$_3$ to 'build up'

298 from hydrolysis of excreted urea before significant emissions occurred. Downwind concentrations (CS1 and

299 CS3) peaked during the next day (19/05), with peak emissions occurring at midday when there was a 5-6 µg m^{-3}

300 horizontal concentration gradient (ΔC) measured between the upwind and downwind receptors. The peak

301 emission rate at this time was around 1.1 µg m^{-2} s^{-1} for both downwind receptors. A decrease in the measured

302 downwind concentrations occurred at 15:00, and an associated decrease in emissions is logically estimated for

303 this time period. The decline in emissions follows 4.4 mm of rain during the day of 19/08, where the rainfall

304 intensity peaked shortly after midday. In addition, the cattle were removed from the field at 15:00; therefore the

305 suspension of excretions to the field and the wet conditions are most likely the dominant factors driving the

306 declining emissions. The LW sensor indicated that the canopy was wet (conductivity reading above baseline) for

307 84% of Period 1 (Table 2).

308 Coinciding with the daytime peak in emissions and downwind concentrations were peaks in T and u, while RH

309 reached a minimum (Figure 4). During the night emissions decreased to near 0, where RH reaches a maximum

310 and T and u reach a minimum. The average Q_{dep} gross emission estimates are greater than the Q net emission

311 estimates by 13-16%.

3.2 Period 2 (20-29/05): grazing on whole field

3.2.1 Concentration measurements

314 Concentration measurements during Period 2 (20-29/05) revealed considerable differences between downwind

315 receptors, where the average CS1 at the center of the field was much greater than the average CS3 at the SE

316 corner (Figure 5), with period averages of 5.6 µg m^{-3} and 3.9 µg m^{-3}, respectively. This may be partially

317   explained by the location of the receptors relative to the grazed field under the prevailing wind conditions.

318   Sensor S1 was located in the center of the field, with an upwind fetch of grazed field across a wider band of

319   wind directions. Sensor S3 on the other hand is located at the SE field boundary, and was more limited as a

320   receptor for emissions under the prevailing northerly wind conditions. However, during NW wind directions

321   where all sensors in-line across a diagonal fetch of the field one would expect the S3 sensor to be measuring

322   similar or higher concentrations relative to S1 at the center (assuming homogenous emissions across the field),

323   which is not the case. It is also important to note that the grazing density was about 50% lower during Period 2

324   as the field was much larger.

325   Power failure led to significant data gaps from the S2 sensor and hence a loss of C_b measurements (Figure 6).

326   To fill the gaps a linear regression applied between the measured S2 concentration and temperature (T), wind

327   speed (u) and relative humidity (RH), however there was considerable scatter in the data and the C_b prediction

328   was much more uncertain than during Period 1.

329    $$C_b = 2.5 - 0.1u + 0.01T - 0.02RH, \text{r2} = 0.1 \qquad (6)$$

330   **3.2.2 Field-scale emissions estimates**

331   The average net emission rate (Q) from the grazed field estimated using the S1 measurements was 0.27 µg m^{-2} s^{-}

332   ^{1} while much lower emissions were estimated from the S3 measurements (0.12 µg m^{-2} s^{-1}). Both estimates show

333   a generally diurnal trend of peak emissions during the afternoon, similar to the trend observed during Period 1.

334   However there are gaps in QS1 and QS3 overnight due to data filtering as $u*$ drops below the defined threshold

335   (0.1 m s^{-1}). Peak emissions occurred on 22/05 when the maximum concentration difference between upwind and

336   downwind receptors was measured. Grazing of the field ended and the cattle left the field at 15:00 GMT on

337   23/05. After this point a generally decreasing trend in emissions is derived from the decreasing concentrations

338   measured by S1 and S3. There is greater uncertainty attributed to the periods without active C_b measurements

339   marked on Figure 6.

340   Emission estimates from the bLS-R model were initially made on the assumption that emissions from the grazed

341   field are spread equally (thus randomly) across a homogeneous field. However a herd of cattle can be expected

342   to move and disperse across the field in a generally non – random way, grouping together as they graze across

343   the field rather than acting individually. Systematic effects of uneven cattle distribution within grazed pastures

344   have been reported previously, impacting on bLS-derived mean gaseous emissions from grazing cattle (Laubach

345   et al., 2013b). Our measurements during Period 2 certainly support spatial heterogeneity in emissions, with

346   higher concentrations at the centre of the field (CS1) than at the SE corner (CS3) during periods where the wind

347   direction was from the NW. Had emissions from the field been homogenous, an increase in NH$_3$ concentration

348   would have been measured across the NW - SE transect of the field.

349   A second set of emission estimates (Figure 6 Panel 3) were produced after optimising the emission rates from 4

350   separate areas (A, B, C & D, Figure 1) within the field to reproduce the observed concentrations at S1 and S3 on

351   each measurement day. An excellent fit between QS1 and QS3 was achieved after running a numerical solver to

352   minimise the squared error (e^2) between them. The coefficients given in Table 1 are the result of the solver,

353   describing the spatial changes in relative emission strength over time. The solver was executed with the

354   following conditions: (1) the sum of the area coefficients must equal 1; and (2) no area coefficient can be below

355   0.075. The minimum value for any area coefficient (AC_{min}) is a parameter which describes the heterogeneity of

356   emissions, where in this case it was assumed that each source area must contribute at least 30% of the original

357   (homogenous) value.

358   Henceforth the initial emission estimates calculated without applying emission area coefficients are referred

359   to as Scenario 1 estimates, while the calculations involving heterogeneous emission area coefficients are referred

360   to as Scenario 2 estimates. It is important to note that there can be more than one combination of coefficients to

361   reconcile the QS1 and QS3 estimates, thus these coefficients should not be taken as definite emission strengths

362   for each area of the field. However they do offer a rough guide to which sections had greater emissions relative

363   to the others, and confirm that emissions from the field were certainly not homogeneous over the course of the

364   grazing period. The large difference in Scenario 1 QS1 and QS3 estimates may therefore be attributed to strong

365   emissions in areas A and D, relative to C and B (Figure 1, Table 1), which explains the high measured

366   concentrations at sensor S1 relative to S3. Emission area D represents the SW field which was grazed during

367   Period 1, thus high emissions from this area may have been a legacy effect left by continuing emissions from

368   cattle excretions during Period 1. Emission area D also contained a water trough which was only 15-20m away

369   from the S1 receptor, where cattle grouping was observed. Due to the combined effects of prior grazing within

370   the SW field and grouping around the water trough, we can expect enhanced emissions within area D. The

371   Scenario 2 (optimised) QS1 and QS3 estimates are similar (0.19 and 0.16 µg m^{-2} s^{-1} respectively), and are

372   believed to give a more realistic estimate of the true field-scale emission rates after accounting for spatial

373   complexity. The data coverage for QS3 (64%) is greater than the QS1 data coverage (59%), hence some

374   differences between QS1 and QS3 can be expected even with perfect agreement. The Q estimates can be

375   regarded as net emission rates for the grazed field, made without consideration of deposition to clean patches

376   within the source area. The Q_{dep} estimates including the effect of deposition are 16% higher (0.22 and 0.19 µg

377   m^{-2} s^{-1} for the Scenario 2 S1 and S3 estimates respectively).

378   **3.3 Derived emission factors**

379   Grazing Period 1 took place within a SW section of the field with a smaller area (5600 m^2) than the whole field

380   opened up for grazing Period 2 (19800 m^2). Although there were fewer cattle grazing during Period 1 (25) the

381   grazing density was twice as high relative to Period 2. Therefore the higher grazing density during Period 1 is

382   consistent with the stronger emission estimates per unit area (Table 2). Emission factors (EFs) are given in

383   Table 3 for Periods 1 and 2. For both measurement periods, the S3 sensor had greater data coverage than the S1

384   sensor. Therefore, the S3 emission estimates are more representative and are selected to derive EFs. Both

385   grazing periods have produced similar emission factors of the order of 6-7 g NH$_3$ cow^{-1} d^{-1}, though there are

386   considerable differences between the two periods in terms of weather conditions and grazing timeline. Period 1

387   was shorter in length, and was characterised by steady SW/W winds, lower temperatures and wetter conditions

388   relative to Period 2 (Table 2). Therefore, the lower temperatures and wetter conditions likely limited emissions

389   (e.g. Flechard et al., 1999; Laubach et al., 2012; Móring et al., 2016).

390   The duration of Period 1 was too short to fully capture tailing emissions, while excretions to the field during

391   Period 1 will have continued to emit NH$_3$ during Period 2. Flux estimates are continued for 6 days after the

392   cattle had left the field during Period 2, capturing residual emissions after grazing. The combined influences of

393   weather conditions and experimental design and duration may therefore explain why a smaller fraction of

394   excreted N and urine-N was emitted as NH$_3$ during Period 1 relative to Period 2. The EFs derived from Period 2

395 fluxes may for these reasons be considered to be more representative of the total emissions from grazing, where

396 emissions are estimated to be 6 and 7 g NH$_3$ cow^{-1} d^{-1}, and 9 and 10% excreted urine-N emitted as NH$_3$ for the Q

397 and Q_{dep} scenarios respectively. However, the greater uncertainty in Period 2 associated with missing C_b

398 measurements and heterogeneous emission patterns should be considered.

4. Discussion

4.1 Experimental design

401 Previous experiments to deduce surface-air fluxes by the bLS method have deployed sufficient measurement

402 systems so that the problem to determine C and C_b was mathematically over-determined, and the experiment

403 was not dependent on a specific range of wind directions (e.g. Flesch et al., 2014). The configuration of the

404 three miniDOAS sensors and the grazed field during Period 2 led to certain wind directions being unsuitable for

405 emission estimates, while additional miniDOAS sensors placed at field boundaries would have been beneficial.

406 However, the configuration of the miniDOAS sensors was optimised by using the weather forecast to predict the

407 wind direction prior to the grazing experiment and placing the miniDOAS sensors accordingly.

408 It was originally hypothesised that the model could treat the field area as a spatially homogenous source, where

409 emission estimates would show insensitivity to cattle grouping and excretion patterns within the field. This

410 assumption seemed valid for the Period 1 emission estimates, where very good agreement was achieved in C

411 and Q between the downwind receptors. The SW field grazed during Period 1 was smaller than the whole field

412 grazed during Period 2, and the wind direction was more consistent. This allowed the downwind and upwind

413 receptors to capture the inflow and outflow concentrations and produce reliable emission estimates, while the

414 grazing density was higher. During Period 2 the field was larger and the grazing density was 50% lower, which

415 led to some spatial and temporal emission 'hotspots' caused by cattle grouping and/or excretions within certain

416 areas, such as around the water trough. The S1 sensor was located very close to a particular 'hotspot' of

417 emissions at the centre and SW section of the field, while the S3 sensor was located next to an area (SE corner)

418 which appears to have seen relatively little emissions. Because of this the model could not treat the field as a

419 homogenous source area and reconcile emission estimates between downwind receptors, and source-area

420 differentiation (Table 1) was required. Therefore there is a limitation in the application of the standard bLS

421 method to estimate emissions from area sources which may not be treated as homogenous, such as pastures with

422 a low grazing density. However as the Period 2/Scenario 2 emission estimates demonstrate it may also be

423 possible to account for this heterogeneity if more than one downwind concentration receptor is used and they are

424 suitably located. Insensitivity to heterogeneous emissions has been demonstrated if concentration measurements

425 are made at least twice as far downwind as the maximum distance between potential sources (Flesch et al.,

426 2005). Therefore had the miniDOAS sensors been placed differently to satisfy this criterion it is possible that no

427 source area optimisation would have been necessary to reconcile bLS emission estimates. However, as

428 emissions from excretions to the grazed pasture were relatively weak, at a greater distance downwind from the

429 field the concentration rise above background may not be significant enough to evaluate the emissions.

430 Felber et al., (2015) applied corralling of grazing cattle into paddocks over a rotational grazing cycle to increase

431 grazing density, and placed GPS trackers on individual cattle to attribute eddy covariance methane fluxes using

432 a footprint model. The Period 1 emission estimates demonstrate that a smaller paddock and higher grazing

433 density can be a solution to the heterogeneous emissions problem, however NH_3 emissions from grazing cattle

434 arise from excretions to the field surface and are not enteric, hence GPS trackers on cattle may not track the NH_3

435 emissions directly as they do for methane. In order to accurately attribute fluxes from grazed pastures there is

436 call to develop a method to track excretions spatially and temporally across a grazed field, potentially using

437 visual observations or cameras and animal detection software. We did carry out visual observations of urination

438 events during Period 1 (day time only), which described a fairly homogenous distribution (data not shown, Andi

439 Móring, personal communication). However observations were not carried out during Period 2.

4.2 Uncertainty in field-scale emission estimates

4.2.1 Uncertainty in miniDOAS concentration measurements and dispersion model

442 The instrumental uncertainty associated with the miniDOAS concentration measurements was evaluated during

443 the initial inter-comparison phase, where the systems were configured to measure in parallel. Very good

444 agreement was observed between the analysers, with a slope of one and an intercept close to zero. Deviations

445 between the S1, S2 and S3 analysers were minor, and the coefficient of variation between them was determined

446 to be 3.4% (unpublished data). Sintermann et al. (2016) have described this inter-comparison phase and the

447 miniDOAS performance in detail.

448 Since the input data had been filtered to remove conditions which do not meet the established criteria ($u* < 0.1$

449 m s^{-1}), and instrumental uncertainty associated with the concentration measurements is very low, the principal

450 uncertainties are associated with the modelled results, principally the input variables which could not be

451 measured directly, such as R_c, and the predicted background concentration C_b used for gap-filling.

452 The bLS dispersion model theory has been well validated in past experiments (e.g. Flesch et al., 2004; McGinn

453 et al. 2009), however we can assume a general overall uncertainty based on evaluated performance by an

454 ensemble of published trace gas release experiments. A review of 24 bLS tracer release assessments (Häni et al.,

455 2016) found that the uncertainty is generally between 10 and 20% for the bLS method.

4.2.2 Uncertainty in background concentration

457 The background concentration (C_b) had to be predicted to "fill in" the gaps in the C_b measurements upwind of

458 the field measured by miniDOAS sensor S2. Multiple regression equations (Eq. 5; 6) were based on previous

459 observations that background NH_3 is dependent on wind speed, temperature and relative humidity (Flechard and

460 Fowler, 1998), but nonetheless error is introduced due to differences between the predicted C_b and the actual C_b.

461 The mean absolute error (MAE) between the measured and predicted C_b for Periods 1 and 2 have been applied

462 to offset to the predicted C_b timeseries input to the model, to determine the limits (upper and lower) of emission

463 estimates caused by this uncertainty. The MAE between the observed and predicted background concentrations

464 during Period 1 was 0.33 µg m^{-3}, while the percentage of data coverage (observed C_b measurements) was 67%.

465 Measurement Period 2 had a greater MAE between observed and predicted C_b (0.56 µg m^{-3}) (Table 4), as the

466 multiple regression equation used to fill (C_b) measurement gaps did not give very accurate predictions (Eq. 6).

467 Furthermore, the upwind sensor S2 was only active during 44% of the measurement period; therefore the Period

468 2 emission estimates are more sensitive to this uncertainty. The % change in Q_{dep} to predicted $C_b \pm$ MAE was

469 much greater during Period 2 ($\pm$ 31%) than Period 1 ($\pm$ 5%).

4.2.3 Uncertainty in local dry deposition of field-emitted NH$_3$

The inclusion of dry deposition within the bLS-R model is intended to simulate the deposition of NH$_3$ to the surface of 'clean' grass patches within the grazed field. This process is described by a resistance model, and while the R_a and R_b components may be derived directly from eddy covariance measurements, as well as well-established models, the R_c component is empirical. In this case, the empirical R_c model (Eq. 4) was derived from a curve fitting exercise of time-integrated COTAG flux measurement to meteorological variables T and RH. The R_c model is based on a long (1.5 years) series of measurements taken from the field (deposition periods only), while the effect of soiled grass areas on R_c during grazing is also approximated using the 130 s m^{-1} R_c offset within the Q_{dep} scenario. It is conceivable that there is significant error (up to 50%) in estimating R_c by this method. The sensitivity of the bLS-R model to potential uncertainty within the R_c estimates has been evaluated, where the R_c timeseries has been varied by factors of plus and minus 50%. The results of this sensitivity test are given in Table 4. The % change in Q_{dep} after varying R_c by $\pm$ 50% was -4% and +12% for Period 1 and $\pm$ 5% for Period 2.

While impact of this uncertainty on the absolute value for Q_{dep} is not very large, the change in Q_{dep} relative to Q is significant. The Period 2 Q_{dep} uncertainty due to predicted R_c is $\pm$ 5%; therefore including deposition in the model has increased Q_{dep} above Q by 16 $\pm$ 6%. Alternatively, we can say that 14 $\pm$ 4% of NH$_3$ emitted from excretions had been re-deposited to clean patches on the field.

4.2.4 Uncertainty associated with heterogeneous emission patterns

To address the resulting disparity between emission estimates from the downwind concentration receptors during Period 2, the emission area coefficients (Table 1) were applied to reconcile the independent emission estimates. This is a valid approach to describe emissions from the field as a whole, as sensor S1 was placed at the center of the field near the strongest area of emissions, causing emissions to be overestimated as a whole, while the field area around sensor S3 at the SE corner seems to have contributing very little emissions, hence causing an underestimation. However, as mentioned previously there are multiple configurations of source area coefficients which can reconcile $QS1$ and $QS3$. Therefore a sensitivity test has been carried out to evaluate the potential error in this method. The numerical solver which derives the source area coefficients contains a parameter assuming the maximum degree of heterogeneity for the field, where each source area cannot contribute less than a defined percentage to the overall emissions. This parameter (AC_{min}) was varied to provide differing sets of source area coefficients, yet still reconciling the $QS1$ and $QS5$ emission estimates which was a necessary precondition for the sensitivity test. AC_{min} was initially assumed be 0.075, 30% of the value for a homogenous field (0.25), and this value was varied by $\pm$ 67% (to 50% and 10% of the homogenous value). The results of this sensitivity test are given in Table 4, where the percentage change in Q_{dep} after varying the parameter by +67% and -67% was 9 and 1, respectively. The percentage change is greater after increasing AC_{min} because $QS1$ and $QS3$ cannot be reconciled as closely, whereas decreasing AC_{min} from 0.075 leads to very little change as the numerical solver can find very close agreement. This suggests that emissions from excretions to the field are too heterogeneous to assume an AC_{min} value of 0.125 (50% of homogeneous value), and that the 1% change in Q_{dep} after reducing AC_{min} to 0.025 (10% of homogeneous value) is more indicative of the uncertainty in the source area optimisation method.

508   The % change in emission estimates was much more sensitive to uncertainty in predicted C_b than to uncertainty

509   in R_c or AC_{min}. Therefore we expect predicted C_b to be the greatest source of error in derived fluxes from the

510   grazed field.

511   **4.3 Temporal variability in estimated emissions**

512   The estimated emissions show significant temporal variability during both measurement periods, typically with

513   peak emissions occurring during the day with little emissions occurring overnight. Similar diurnal profiles have

514   been observed in NH_3 emissions from cattle urine and dung patches (Laubach et al., 2012; 2013a), and from

515   urine patch emission models (Móring et al., 2016). Mechanisms which limit nocturnal emissions can be

516   summarised as: (1) low wind speeds and stable conditions, which increases the aerodynamic transfer resistances

517   between the soil/canopy layer and the atmosphere, (2) low temperatures which limit the hydrolysis of urea, and

518   affect NH_3/NH_4^+ partitioning in solutions, (3) dew formation on leaf surfaces which act as sinks for NH_3.

519   A longer temporal trend in emissions is observed during Period 1; with very little emissions occurring on the

520   first day the cattle were introduced to the field, and peak emissions occurring during the afternoon of the second

521   day. After 44 cattle had begun to graze the whole field during Period 2, peak emission rates occurred from 22-

522   23/05, 2-3 days after the cattle had been introduced. A decreasing trend in emissions occurred after the cattle

523   were removed from the field on 23/05 until the end of the measurement period. This is in-line with the reported

524   emissions from urine and dung patches by Laubach et al., (2013a), where emissions peaked during the third and

525   fourth days after grazing had begun, and a following decreasing trend in emissions after the cattle had been

526   removed from the field on the third day.

527   The peak in emissions which occurred during grazing can be attributed to the hydrolysis of urea within the urine

528   patches, which leads to a rapid rise in pH and the formation of NH_4^+, and a high rate of NH_3 volatilisation

529   (Sherlock and, Goh 1985). As volatilisation proceeds, a subsequent chemical reduction in surface pH occurs

530   with an accompanying release of a proton to the transformation of NH_4^+ to NH_3 (Laubach et al., 2012; Sherlock

531   and Goh, 1985, Móring, et al. 2016), which prevents further volatilisation and can explain the declining

532   emission rate after the cattle had left the field on 23/05.

533   **4.4 Emission factors from the grazing experiment**

534   Emission factors from the grazing experiment have been evaluated as 6 ± 2 and 7 ± 2 g NH_3 cow^{-1} d^{-1}, and 9 ±

535   3% and 10 ± 3% of excreted urine-N emitted as NH_3 for the Q and Q_{dep} scenarios respectively (average

536   emission factor ± predicted C_b uncertainty). These emission factors were taken from the Period 2/Scenario 2

537   estimates as Period 1 was not long enough to fully capture emissions from excretions to the field. Previous

538   experiments have measured NH_3 emissions from cattle urine patches at ratios of 7-25.7% of excreted urine-N to

539   grazed pastures (Jarvis et al., 1989; Ryden et al., 1987; Laubach et al., 2012; 2013a). Our estimates for

540   emissions from grazing are towards the lower end of the range of published emission factors. Differences

541   between reported emission factors may be related to differing weather conditions affecting the hydrolysis of

542   urea, or differences in soil properties, where emissions can be limited due to urine percolation into porous soil

543   (Móring et al., 2016). It is also possible that significant emissions occurred after the miniDOAS instruments had

544   been removed from the field, which would lead to an underestimation of the proportion of excreted N or urine-N

545   emitted as NH_3. The period of significant emissions from urine patches generally lasts 4-8 days after urine

546   deposition (Sherlock and Goh, 1985; Laubach et al., 2012). However, a rainfall event after a dry period can lead

547   to a delayed onset of NH_3 emissions by restarting urea hydrolysis (Móring et al., 2016). On the other hand, the

548   Period 2 emission factors are also influenced to some degree by emissions from excretions during Period 1 on

549   the SW field, which could cause an overestimation of emissions. Emission factors derived from Period 2 are

550   also affected by $u*$ filtering, which may slightly increase estimates due to a measurement bias towards

551   turbulent daytime periods.

552   The emission estimates presented here show that the 'gross' emissions from the field (Q_{dep} scenario) are around

553   $16 \pm 6\%$ higher than the 'net' emissions (Q scenario). Both of these estimates are potentially useful to contribute

554   towards an emission factor for livestock grazing. For example, regional-scale atmospheric dispersion models

555   may require source inputs as 'gross' emission factors due to deposition simulations implicit within the regional-

556   scale model.

557   **5. Conclusion**

558   Fluxes of NH_3 were estimated through measurement of atmospheric concentrations upwind and downwind of a

559   grazed field, and applying a bLS dispersion model to simulate the emission rate on a half hourly basis from the

560   observed horizontal concentration gradient and wind/turbulence measurements. The miniDOAS systems were

561   well-suited to the task, providing continuous high-time resolution concentration measurements at field

562   boundaries across the field. Horizontal concentration gradients of ~0-9 µg m^{-3} were measured between upwind

563   and downwind receptors. Control on emissions was observed from covariance with temperature, wind speed and

564   humidity/wetness measurements made on the field, revealing a diurnal emission profile. Two separate

565   experiments to evaluate emissions were carried out; a Period 1 experiment (2 days) which took place on a small

566   field with a grazing density of 44 cows ha^{-1}, and a Period 2 experiment (10 days) on a larger field with a

567   grazing density of 22 cows ha^{-1}. Spatial heterogeneity in emissions across the field was apparent during Period

568   2, as a result of uneven cattle distribution and a low grazing density, adversely affecting the accuracy of the bLS

569   model estimates. However, after treating the larger field as a grid of discrete source areas the spatial

570   heterogeneity of emissions was accounted for, by optimising source area coefficients to the measured

571   concentrations and reconciling emission estimates between downwind receptors.

572   Data gaps in the C_b measurements were filled by applying linear regression equations with u, T and RH, which

573   introduced significant uncertainty into the emission estimates. The evaluated uncertainty in derived emissions

574   due to C_b gap-filling was 5% during Period 1 and 31% during Period 2.

575   In contrast to the standard bLS approach, we simulated the effect of re-deposition to unsoiled field patches,

576   where the canopy resistance (R_c) component was estimated by an empirical model derived from local flux and

577   R_c measurements with T and RH. Including deposition in the model increased emissions by $16 \pm 6\%$. The

578   results present both 'gross' and 'net' emissions from the field, and show that deposition of NH_3 is an important

579   consideration when deriving NH_3 emission factors.

580   **Acknowledgements**

581   This study was undertaken as part of the French BtEP project (Emissions gazeuses au Bâtiment, sTockage,

582   Epandage et Pâturage des systèmes bovins laitiers), convention n° 1360C0032, with funding provided by

583   ADEME (Agence de l'environnement et de la maîtrise de l'énergie). We wish to thank David Sidaner, Jacques
584   Lassalas and all of the staff at the INRA-Méjusseaume dairy experimental farm. We wish to thank Andi Móring
585   for assistance during the measurement campaign. We wish to thank Thomas Kupper for organising the setup of
586   the N excretion model.

587   **Competing interests**

588   The authors declare that they have no conflict of interest.

589   **References**

590   Asman, W. A. H.: Factors influencing local dry deposition of gases with special reference to ammonia,
591   Atmospheric Environment, 32, 415-421, Doi 10.1016/S1352-2310(97)00166-0, 1998.

592   Asman, W. A. H., Sutton, M. A., and Schjorring, J. K.: Ammonia: emission, atmospheric transport and
593   deposition, New Phytol, 139, 27-48, DOI 10.1046/j.1469-8137.1998.00180.x, 1998.

594   Bracher A., Schlegel P., Münger A., Stoll W., Menzi H., 2011. Möglichkeiten zur Reduktion von
595   Ammoniakemissionen durch Fütterungsmassnahmen beim Rindvieh (Milchkuh). Project report Schweizerische
596   Hochschule für Landwirtschaft and Agroscope Liebefeld-Posieux for the Swiss Federal Office of Agriculture,
597   pp. 128, available at: https://www.blw.admin.ch/blw/de/home/instrumente/ressourcen--und-
598   gewaesserschutzprogramm/ressourcenprogramm.html, last access: 4 October 2016.

599   Bracher A., Spring P., Münger A., Schlegel P., Stoll W., Menzi H., 2012. Feeding measures to reduce ammonia
600   emissions. Hassouna M. et al. (Eds), Proc. International Symposium on Emissions of Gas and Dust from
601   Livestock (EMILI), Saint-Malo 11-13.6.2012, p. 39.

602   Carslaw, D. C., and Ropkins, K.: openair - An R package for air quality data analysis, Environ Modell Softw,
603   27-28, 52-61, 10.1016/j.envsoft.2011.09.008, 2012.

604   Erisman, J. W., Sutton, M. A., Galloway, J., Klimont, Z., and Winiwarter, W.: How a century of ammonia
605   synthesis changed the world, Nat Geosci, 1, 636-639, 10.1038/ngeo325, 2008.

606   Famulari, D., Fowler, D., Nemitz, E., Hargreaves, K. J., Storeton-West, R. L., Rutherford, G., Tang, Y. S.,
607   Sutton, M. A., and Weston, K. J.: Development of a low-cost system for measuring conditional time-averaged
608   gradients of SO2 and NH3, Environmental Monitoring and Assessment, 161, 11-27, 10.1007/s10661-008-0723-
609   6, 2010.

610   Felber, R., Munger, A., Neftel, A., and Ammann, C.: Eddy covariance methane flux measurements over a
611   grazed pasture: effect of cows as moving point sources, Biogeosciences, 12, 3925-3940, 10.5194/bg-12-3925-
612   2015, 2015.

613   Flechard, C. R., and Fowler, D.: Atmospheric ammonia at a moorland site. I: The meteorological control of
614   ambient ammonia concentrations and the influence of local sources, Q J Roy Meteor Soc, 124, 733-757, DOI
615   10.1002/qj.49712454705, 1998.

616   Flechard, C. R., Fowler, D., Sutton, M. A., and Cape, J. N.: A dynamic chemical model of bi-directional
617   ammonia exchange between semi-natural vegetation and the atmosphere, Q J Roy Meteor Soc, 125, 2611-2641,
618   DOI 10.1002/qj.49712555914, 1999.

619 Flechard, C. R., Spirig, C., Neftel, A., and Ammann, C.: The annual ammonia budget of fertilised cut grassland
620 - Part 2: Seasonal variations and compensation point modeling, Biogeosciences, 7, 537-556, 2010.

621 Flechard, C. R., Massad, R. S., Loubet, B., Personne, E., Simpson, D., Bash, J. O., Cooter, E. J., Nemitz, E., and
622 Sutton, M. A.: Advances in understanding, models and parameterizations of biosphere-atmosphere ammonia
623 exchange, Biogeosciences, 10, 5183-5225, 10.5194/bg-10-5183-2013, 2013.

624 Flesch, T. K., Wilson, J. D., and Yee, E.: Backward-Time Lagrangian Stochastic Dispersion Models and Their
625 Application to Estimate Gaseous Emissions, J Appl Meteorol, 34, 1320-1332, Doi 10.1175/1520-
626 0450(1995)034<1320:Btlsdm>2.0.Co;2, 1995.

627 Flesch, T. K., Wilson, J. D., Harper, L. A., Crenna, B. P., and Sharpe, R. R.: Deducing ground-to-air emissions
628 from observed trace gas concentrations: A field trial, J Appl Meteorol, 43, 487-502, Doi 10.1175/1520-
629 0450(2004)043<0487:Dgefot>2.0.Co;2, 2004.

630 Flesch, T. K., Wilson, J. D., Harper, L. A., and Crenna, B. P.: Estimating gas emissions from a farm with an
631 inverse-dispersion technique, Atmospheric Environment, 39, 4863-4874, 10.1016/j.atmosenv.2005.04.032,
632 2005.

633 Flesch, T. K., McGinn, S. M., Chen, D., Wilson, J. D., and Desjardins, R. L.: Data filtering for inverse
634 dispersion emission calculations, Agr Forest Meteorol, 198, 1-6, 10.1016/j.agrformet.2014.07.010, 2014.

635 Gao, Z. L., Mauder, M., Desjardins, R. L., Flesch, T. K., and van Haarlem, R. P.: Assessment of the backward
636 Lagrangian Stochastic dispersion technique for continuous measurements of CH4 emissions, Agr Forest
637 Meteorol, 149, 1516-1523, 10.1016/j.agrformet.2009.04.004, 2009.

638 Genermont, S., and Cellier, P.: A mechanistic model for estimating ammonia volatilization from slurry applied
639 to bare soil, Agr Forest Meteorol, 88, 145-167, Doi 10.1016/S0168-1923(97)00044-0, 1997.

640 Gill Instruments: Technical key note KN1509v3* - software bug affecting 'w' wind component notice and
641 available options to customers – February 2016, available at:
642 http://gillinstruments.com/data/manuals/KN1509_WindMaster_WBug_info.pdf, last access: 4 October 2016.

643 Häni, C.: bLSmodelR - An atmospheric dispersion model in R. R package version 2.4.1. URL:
644 http://www.agrammon.ch/documents-to-download/blsmodelr/, last access: 22 September 2016.

645 Häni, C., Sintermann, J., Jocher, M., Neftel, A.: Ammonia emissions after application of slurry. pp. 168.
646 Hochschule für Agrar-, Forst- und Lebensmittelwissenschaften, HAFL, Agroscope Institut für
647 Nachhaltigkeitswissenschaften INH, available at:
648 http://www.agrammon.ch/assets/Downloads/SchlussberichtInklAnh20160728subm.pdf, last access: 4 October
649 2016.

650 Harper, L. A., Denmead, O. T., and Flesch, T. K.: Micrometeorological techniques for measurement of enteric
651 greenhouse gas emissions, Anim Feed Sci Tech, 166-67, 227-239, 10.1016/j.anifeedsci.2011.04.013, 2011.

652 Hertel, O., Reis, S., Skjøth, C. A., Bleeker, A., Harrison, R., Cape, J. N., Fowler, D., Skiba, U., Simpson, D.,
653 Jickells, T., Baker, A., Kulmala, M., Gyldenkaerne, S., Sørensen, L. L., and Erisman, J. W.:, 2011. Nitrogen
654 processes in the atmosphere, in: The European Nitrogen Assessment – Sources, Effects and Policy Perspectives,
655 edited by Sutton, M. A., Howard, C. M., Erisman, J. W., Billen, G., Grennfelt, P., van Grinsven, H., and
656 Grizzetti, B., 177–207, Cambridge University Press, Cambridge, UK, 2011..

657 Hutchings, N. J., Sommer, S. G., Andersen, J. M., and Asman, W. A. H.: A detailed ammonia emission
658 inventory for Denmark, Atmospheric Environment, 35, 1959-1968, Doi 10.1016/S1352-2310(00)00542-2, 2001.

659 Jarvis, S. C., Hatch, D. J., and Roberts, D. H.: The Effects of Grassland Management on Nitrogen Losses from
660 Grazed Swards through Ammonia Volatilization - the Relationship to Excretal-N Returns from Cattle, J Agr Sci,
661 112, 205-216, 1989.

662 Laubach, J., Taghizadeh-Toosi, A., Sherlock, R. R., and Kelliher, F. M.: Measuring and modelling ammonia
663 emissions from a regular pattern of cattle urine patches, Agr Forest Meteorol, 156, 1-17,
664 10.1016/j.agrformet.2011.12.007, 2012.

665 Laubach, J., Taghizadeh-Toosi, A., Gibbs, S. J., Sherlock, R. R., Kelliher, F. M., and Grover, S. P. P.: Ammonia
666 emissions from cattle urine and dung excreted on pasture, Biogeosciences, 10, 327-338, 10.5194/bg-10-327-
667 2013, 2013a.

668 Laubach, J., Bai, M., Pinares-Patino, C. S., Phillips, F. A., Naylor, T. A., Molano, G., Rocha, E. A. C., and
669 Griffith, D. W. T.: Accuracy of micrometeorological techniques for detecting a change in methane emissions
670 from a herd of cattle, Agr Forest Meteorol, 176, 50-63, 10.1016/j.agrformet.2013.03.006, 2013b.

671 Loubet, B., Cellier, P., Milford, C., and Sutton, M. A.: A coupled dispersion and exchange model for short-
672 range dry deposition of atmospheric ammonia, Q J Roy Meteor Soc, 132, 1733-1763, 10.1256/qj.05.73, 2006.

673 Loubet, B., Asman, W. A. H., Theobald, M. R., Hertel, O., Tang, Y. S., Robin, P., Hassouna, M., Dammgen, U.,
674 Genermont, S., Cellier, P., and Sutton, M. A.: Ammonia Deposition Near Hot Spots: Processes, Models and
675 Monitoring Methods, Atmospheric Ammonia, 205-267, Doi 10.1007/978-1-4020-9121-6_15, 2009.

676 McGinn, S. M., Beauchemin, K. A., Flesch, T. K., and Coates, T.: Performance of a Dispersion Model to
677 Estimate Methane Loss from Cattle in Pens, J Environ Qual, 38, 1796-1802, 10.2134/jeq2008.0531, 2009.

678 Menzi H., Huguenin O., Muenger A., Schlegel P. Procedure for defining new Swiss standard values for the
679 nutrient excretions of dairy cows. In Koerner I. et al. (Eds.), Proc. 16th RAMIRAN Conference, Hamburg
680 Harburg September 8-10 2015, Book of Abstracts, p. 52, 2015.

681 Móring, A., Vieno, M., Doherty, R. M., Laubach, J., Taghizadeh-Toosi, A., and Sutton, M. A.: A process-based
682 model for ammonia emission from urine patches, GAG (Generation of Ammonia from Grazing): description and
683 sensitivity analysis, Biogeosciences, 13, 1837-1861, 10.5194/bg-13-1837-2016, 2016.

684 Pain, B. F., Van der Weerden, T. J., Chambers, B. J., Phillips, V. R., and Jarvis, S. C.: A new inventory for
685 ammonia emissions from UK agriculture, Atmospheric Environment, 32, 309-313, Doi 10.1016/S1352-
686 2310(96)00352-4, 1998.

687 R Core Team: R: A language and environment for statistical computing. R Foundation for Statistical
688 Computing, Vienna, Austria, available at: https://www.R-project.org/, last access: 04 October 2016.

689 Reidy, B., Dammgen, U., Dohler, H., Eurich-Menden, B., van Evert, F. K., Hutchings, N. J., Luesink, H. H.,
690 Menzi, H., Misselbrook, T. H., Monteny, G. J., and Webb, J.: Comparison of models used for national
691 agricultural ammonia emission inventories in Europe: Liquid manure systems, Atmospheric Environment, 42,
692 3452-3464, 10.1016/j.atmosenv.2007.04.009, 2008.

693 Ryden, J. C., Whitehead, D. C., Lockyer, D. R., Thompson, R. B., Skinner, J. H., and Garwood, E. A.:
694 Ammonia Emission from Grassland and Livestock Production Systems in the Uk, Environ. Pollut., 48, 173-184,
695 Doi 10.1016/0269-7491(87)90032-7, 1987.

696 Sherlock, R. R., and Goh, K. M.: Dynamics of Ammonia Volatilization from Simulated Urine Patches and
697 Aqueous Urea Applied to Pasture .1. Field Experiments, Fert Res, 5, 181-195, Doi 10.1007/Bf01052715, 1984.

Sherlock, R. R., and Goh, K. M.: Dynamics of Ammonia Volatilization from Simulated Urine Patches and Aqueous Urea Applied to Pasture .2. Theoretical Derivation of a Simplified Model, Fert Res, 6, 3-22, Doi 10.1007/Bf01058161, 1985.

Sintermann, J., Neftel, A., Ammann, C., Hani, C., Hensen, A., Loubet, B., and Flechard, C. R.: Are ammonia emissions from field-applied slurry substantially over-estimated in European emission inventories?, Biogeosciences, 9, 1611-1632, 10.5194/bg-9-1611-2012, 2012.

Sintermann, J., Dietrich, K., Hani, C., Bell, M., Jocher, M., and Neftel, A.: A miniDOAS instrument optimised for ammonia field measurements, Atmos Meas Tech, 9, 2721-2734, 10.5194/amt-9-2721-2016, 2016.

Sommer, S. G., Sogaard, H. T., Moller, H. B., and Morsing, S.: Ammonia volatilization from sows on grassland, Atmospheric Environment, 35, 2023-2032, Doi 10.1016/S1352-2310(00)00428-3, 2001.

Sutton, M. A., Fowler, D., and Moncrieff, J. B.: The Exchange of Atmospheric Ammonia with Vegetated Surfaces .1. Unfertilized Vegetation, Q J Roy Meteor Soc, 119, 1023-1045, DOI 10.1002/qj.49711951309, 1993.

Sutton, M. A., Howard, C. M., Erisman, J.W., Bealey,W. J., Billen, G., Bleeker, A., Bouwman, A. F., Grennfelt, P., van Grinsven, H. and Grizzetti, B.: The challenge to integrate nitrogen science and policies: the European Nitrogen Assessment approach, in: The European Nitrogen Assessment: Sources, Effects and Policy Perspectives, edited by: Sutton, M. A., Howard, C. M., Erisman, J. W., Billen, G., Bleeker, A., Grennfelt, P., van Grinsven, H., and Grizzetti, B., Cambridge University Press, Cambridge, ISBN 978-1-107-00612-6, 82-96, 2011.

Tang, Y. S., Cape, J. N. and Sutton, M. A.: Development and Types of Passive Samplers for 570 Monitoring Atmospheric NO2 and NH3 Concentrations, Sci. World, 1, 513–529, Doi:10.1100/tsw.2001.82, 2001.

Volten, H., Bergwerff, J. B., Haaima, M., Lolkema, D. E., Berkhout, A. J. C., van der Hoff, G. R., Potma, C. J. M., Kruit, R. J. W., van Pul, W. A. J., and Swart, D. P. J.: Two instruments based on differential optical absorption spectroscopy (DOAS) to measure accurate ammonia concentrations in the atmosphere, Atmos Meas Tech, 5, 413-427, 10.5194/amt-5-413-2012, 2012.

von Bobrutzki, K., Braban, C. F., Famulari, D., Jones, S. K., Blackall, T., Smith, T. E. L., Blom, M., Coe, H., Gallagher, M., Ghalaieny, M., McGillen, M. R., Percival, C. J., Whitehead, J. D., Ellis, R., Murphy, J., Mohacsi, A., Pogany, A., Junninen, H., Rantanen, S., Sutton, M. A., and Nemitz, E.: Field inter-comparison of eleven atmospheric ammonia measurement techniques, Atmos Meas Tech, 3, 91-112, 10.5194/amt-3-91-2010, 2010.

Whitehead, D. C.: Grassland Nitrogen. CAB International, Wallingford, UK, 1995.

Zaman, M., Saggar, S., Blennerhassett, J. D., and Singh, J.: Effect of urease and nitrification inhibitors on N transformation, gaseous emissions of ammonia and nitrous oxide, pasture yield and N uptake in grazed pasture system, Soil Biol Biochem, 41, 1270-1280, 10.1016/j.soilbio.2009.03.011, 2009.

731

732

Tables

Table 1: Series of emission coefficients obtained by numerical solving of the difference between $QS1$ and $QS3$, applied to individual emission areas to fit the bLS-R model to concentration measurements on each day. For a grazed field with homogeneous emissions the emission coefficients for each area would be 0.25. Therefore the emission coefficients offset the bias in emission estimates between the sensors S1 and S3 by adjusting to the heterogeneity in emissions across the field area.

Emission area	20/05	21/05	22/05	23/05	24/05	25/05	26/05	27/05	28/05	29/05
A	0.56	0.31	0.28	0.56	0.36	0.42	0.26	0.21	0.25	0.17
B	0.08	0.14	0.13	0.17	0.18	0.17	0.25	0.25	0.23	0.25
C	0.07	0.07	0.20	0.09	0.19	0.11	0.23	0.28	0.21	0.27
D	0.29	0.47	0.40	0.18	0.26	0.30	0.27	0.26	0.31	0.31

739

740

741

742

743

744

745

746

747

748

749

750

751

752

753

754

755

756

757

758

759

760

761

762

763

764

765

766

767

768 **Table 2: Summary table of measurement and modelling results.**

		Period 1			Period 2	
	Scenario[1]	S1	S3	Scenario	S1	S3
$C - C_b$ (µg NH$_3$ m^{-3})		1.4	2.1		2.9	1.2
Q (µg NH$_3$ m^{-2} s^{-1})		0.27	0.29	1	0.27	0.12
				2	0.19	0.16
Q_{dep} (µg NH$_3$ m^{-2} s^{-1})		0.31	0.34	1	0.31	0.14
				2	0.22	0.19
Q_{depmax} (µg NH$_3$ m^{-2} s^{-1})		0.33	0.38	1	0.33	0.14
				2	0.24	0.2
T (°C)		10			14	
u (m s^{-1})		2			1.2	
RH (%)		77			76	
Total Rain (mm)		4.4			0	
LW (% time wet)		84			40	
R_c (s m^{-1})	Q_{depmax}	145		Q_{depmax}	208	
	Q_{dep}	275		Q_{dep}	338	
v_d (mm s^{-1})	Q_{depmax}	4.4		Q_{depmax}	3.2	
	Q_{dep}	2.8		Q_{dep}	2.2	

[1]Description of model scenarios: Q_{dep} is the bLS-R emission estimate including dry deposition, with an offset of 130 s m^{-1} applied to the R_c timeseries to account for the limiting of excreted NH$_3$ to deposition. Q_{depmax} is the emission estimate without the offset applied to the R_c timeseries, and is hence a maximum prediction of the gross emissions from the field. Period 2 emission estimates contain both the original Scenario 1 emission estimates assuming a homogenous field, and the optimised Scenario 2 emission estimates using the area coefficients given in Table 1.

769

770

771

772

773

774

775

776

777

778

779 **Table 3: N excretion model inputs, results, and derived emission factors**

Model Input	Value		Model Output or Emission Factor[1]	Scenario[2]	Value	
	Period 1	Period 2			Period 1	Period 2
Animal Numbers	25	44	N excretion total (kg)		11	40
Animal weight (kg)	650	650	N excretion urine (kg)		8	28
Days since calving	180	183	N excretion faeces (kg)		3	12
Milk yield (kg cow^{-1} day^{-1})	21	22	EF (% total excreted N emitted as NH$_3$)	Q	2.5	5.2
				Q_{dep}	2.9	6
Grass sward: net energy for lactation (MJ kg DM^{-1})	6.4	6.4	EF (% total excreted urine-N emitted as NH$_3$)	Q	2.9	8.9
				Q_{dep}	4.2	10.4
Grass sward: crude protein content (g kg DM^{-1})	168	168	EF (g NH$_3$ cow^{-1} d^{-1})	Q	5.7	6.2
				Q_{dep}	6.5	7.2

[1]N excretion calculations are given as the herd total for each measurement period.

[2]Q is the net emission rate derived without including deposition in the bLS-R simulation, Q_{dep} is the gross bLS-R emission estimate including dry deposition, with an R_c offset of 130 s m^{-1}. EFs are derived from the S3 flux estimates due to better data coverage during both measurement periods, and Period 2 fluxes are derived from Scenario 2 estimates.

780

781 **Table 4: Sensitivity analysis of the percentage change of the bLS-R gross emission estimates (Q_{dep}) to variation in**
782 **predicted C_b and R_c, and the source area coefficient parameter AC_{min}.**

	Period 1	Period 2
C_b data coverage (%)	67	44
C_b MAE (µg m^{-3})	0.33	0.56
% Change C_b ± MAE[1]	-5% +5%	-31% +31%
% Change R_c ± 20%	-2% +3%	-3% +3%
% Change R_c ± 50%	-4% +12%	-5% +5%
% Change AC_{min} ± 67%[2]	-	-9% -1%

[1]The predicted C_b timeseries input to the bLS-R model is varied by the Mean Absolute Error (MAE) between the measured and predicted C_b. The first value in all cases the % change + variation and the second the % change – variation.

[2] The percentage change in Q_{dep} is given after varying the source area coefficient parameter AC_{min} by 67% (0.075 ± 0.05).

783

784
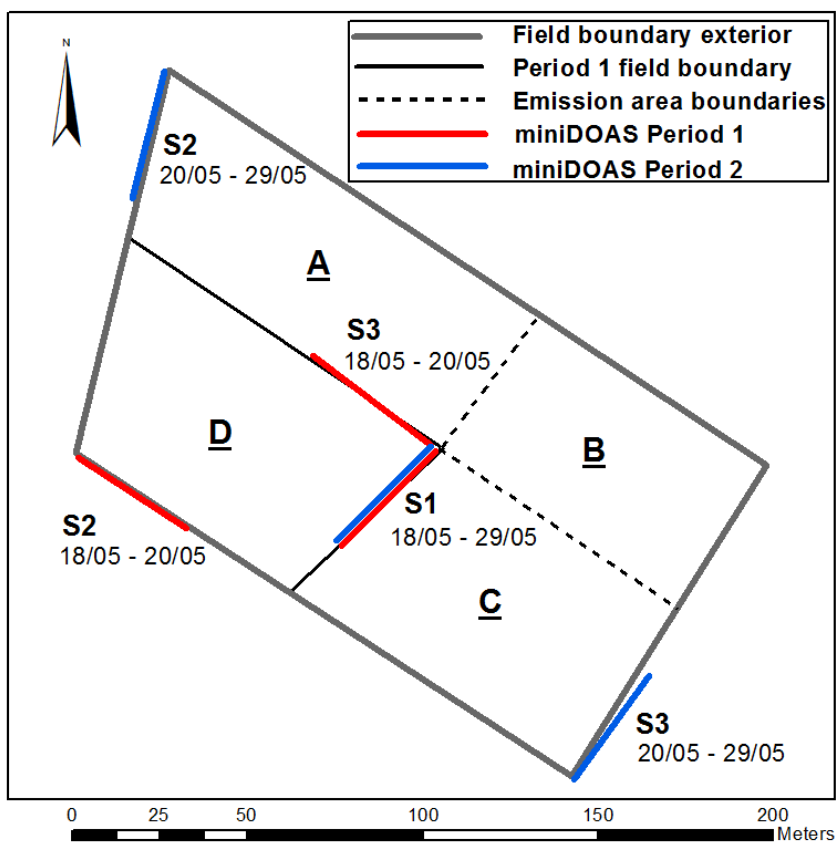
Figures

Figure 1: Map of the grazed field showing positions of the three miniDOAS open-path measurement systems. During Period 1 (18-20/05) 25 cattle were fenced within the SW field section (area D). During Period 2 (20-29/05) the internal field boundaries were removed so that the cattle could graze the whole field. Later, for the attribution of emissions across the field, emission area quadrants have been allocated, marked A-D. There were no physical barriers between the emission areas during Period 2.

792

793

794
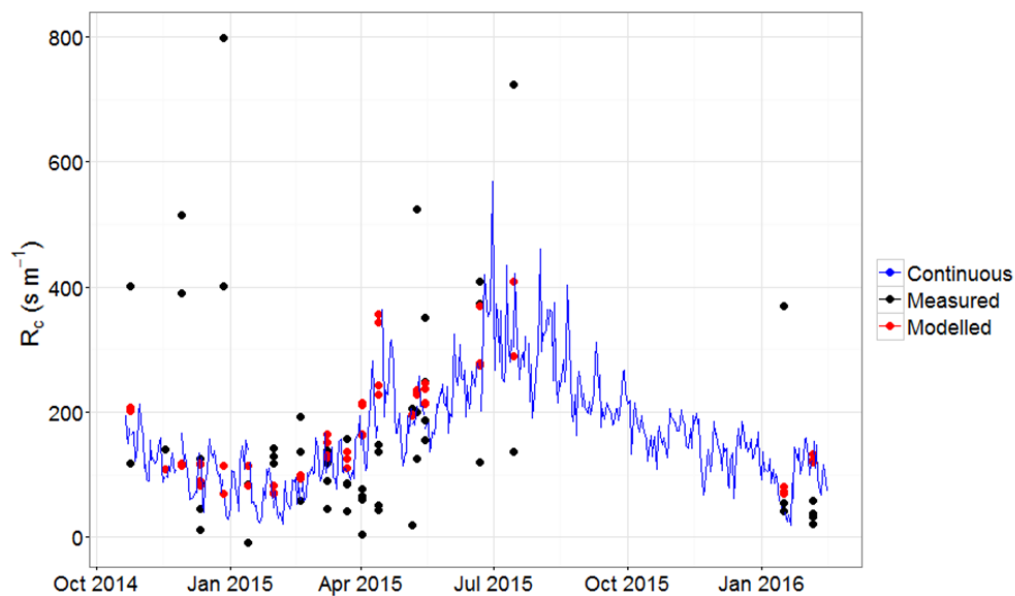
**Figure 2: Timeseries of time-integrated COTAG R_c measurements and Equation 4 R_c estimates. The blue line
represents continuous R_c estimates calculated from the daily mean T and RH measurements at the field site. Black
points are the measured R_c values from the COTAG systems, and the red points are the modelled R_c from the same
time-integrated data.**

799

800
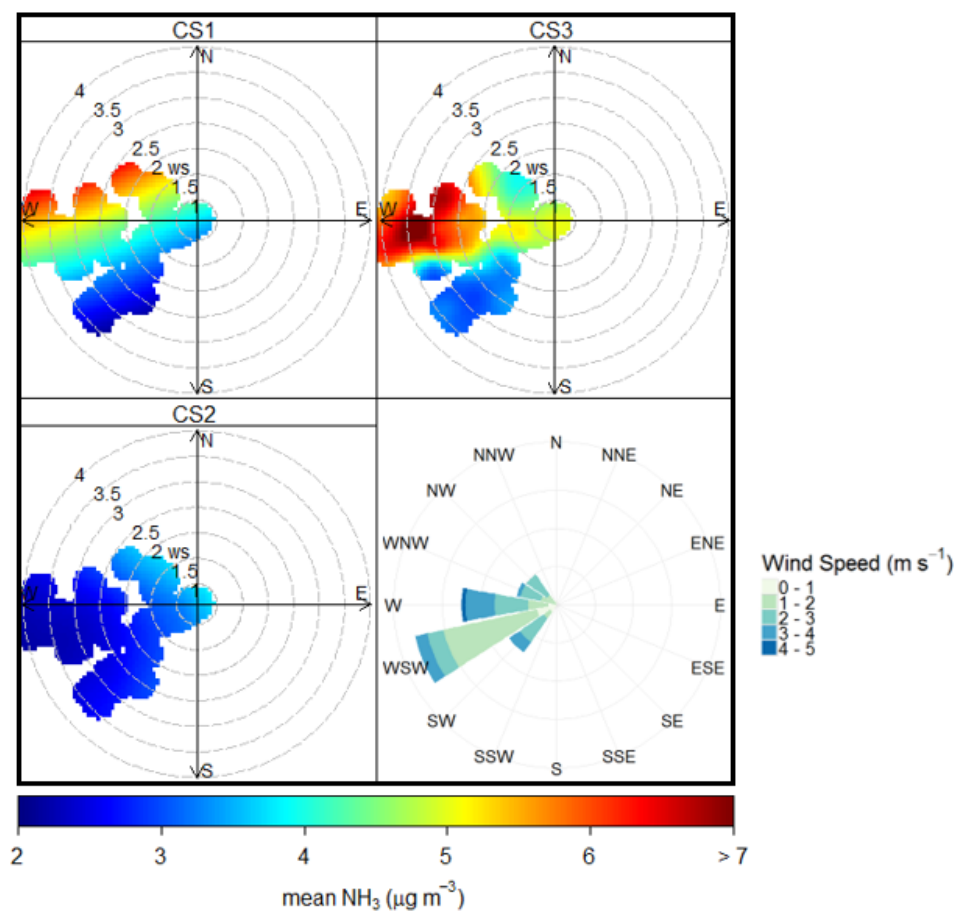
Figure 3: Polar plots showing averaged NH₃ concentrations (colour axis) as a function of wind speed (radial axis) and wind direction (cardinal direction) for each miniDOAS system, and a windrose showing the prevailing wind direction, Period 1 (18-20/05). The concentration Polar plots were produced using the OpenAir R package (Carslaw et al., 2014).

801
802
803
804

805

806

807

808

809

810

811

812

813

814

815
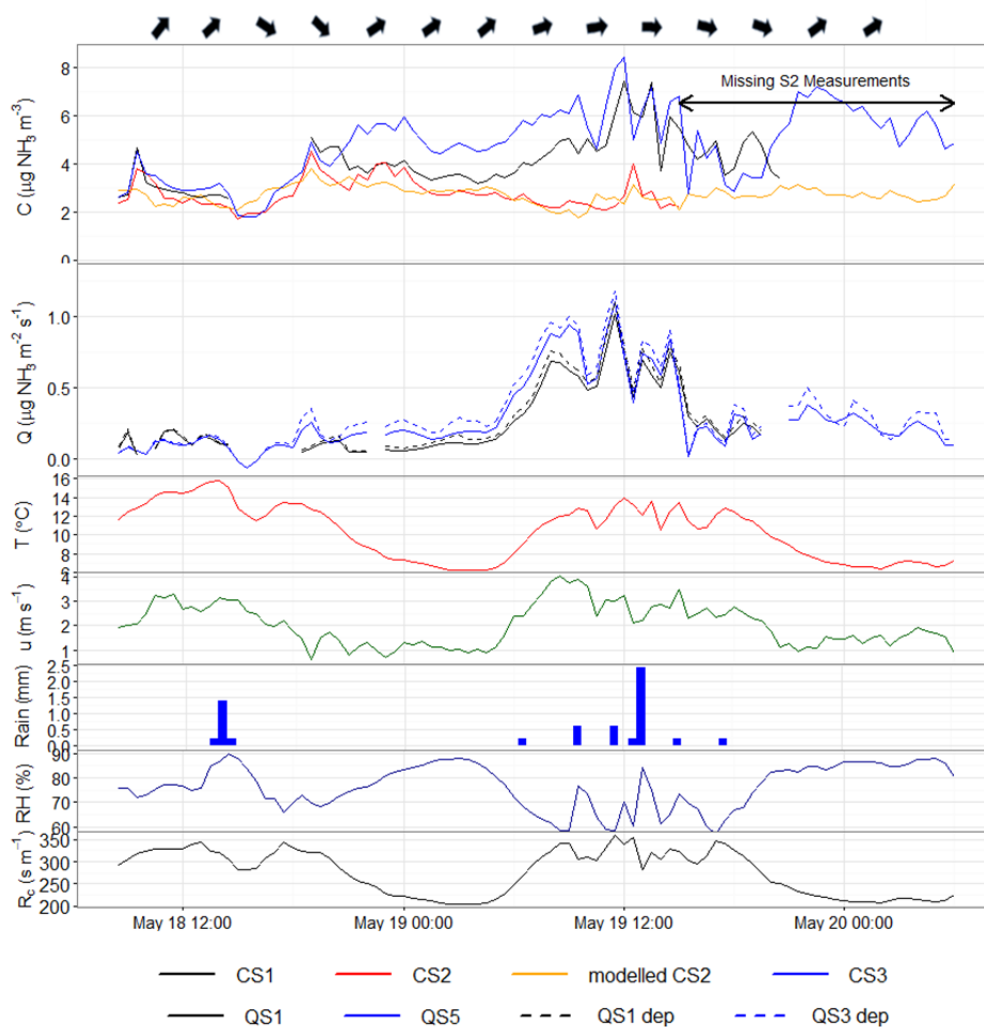
Figure 4: Timeseries of Period 1 DOAS concentration measurements (CS1, CS2, CS3, and modelled CS2 using Equation 6, top panel) and bLS-R emission estimates (Q and Q_{dep} scenarios, second panel), with T, u, Rain, RH, and modelled R_c using Equation 5 shown in the panels below. Wind direction arrows are set above the top panel to visualise changes over time.

820
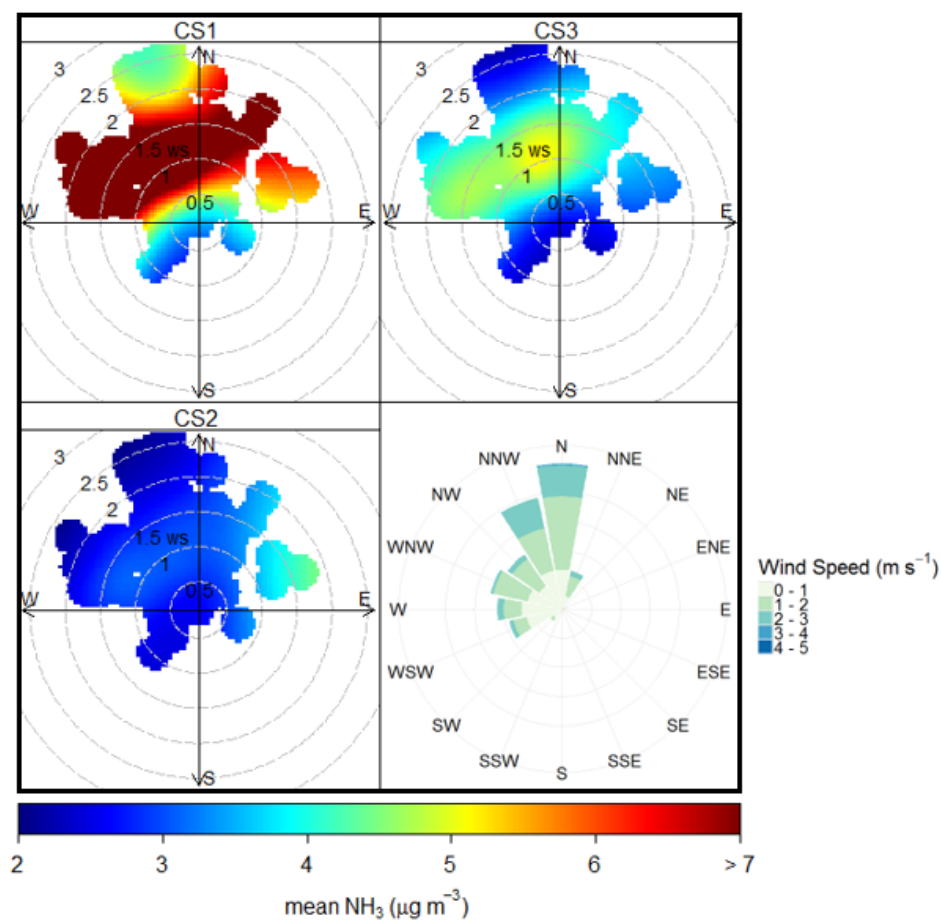
821   **Figure 5: Polar plots showing averaged NH₃ concentrations with wind speed and direction for each DOAS system,**
822   **with a windrose showing the prevailing wind directions, Period 2 (20-29/05).**

823
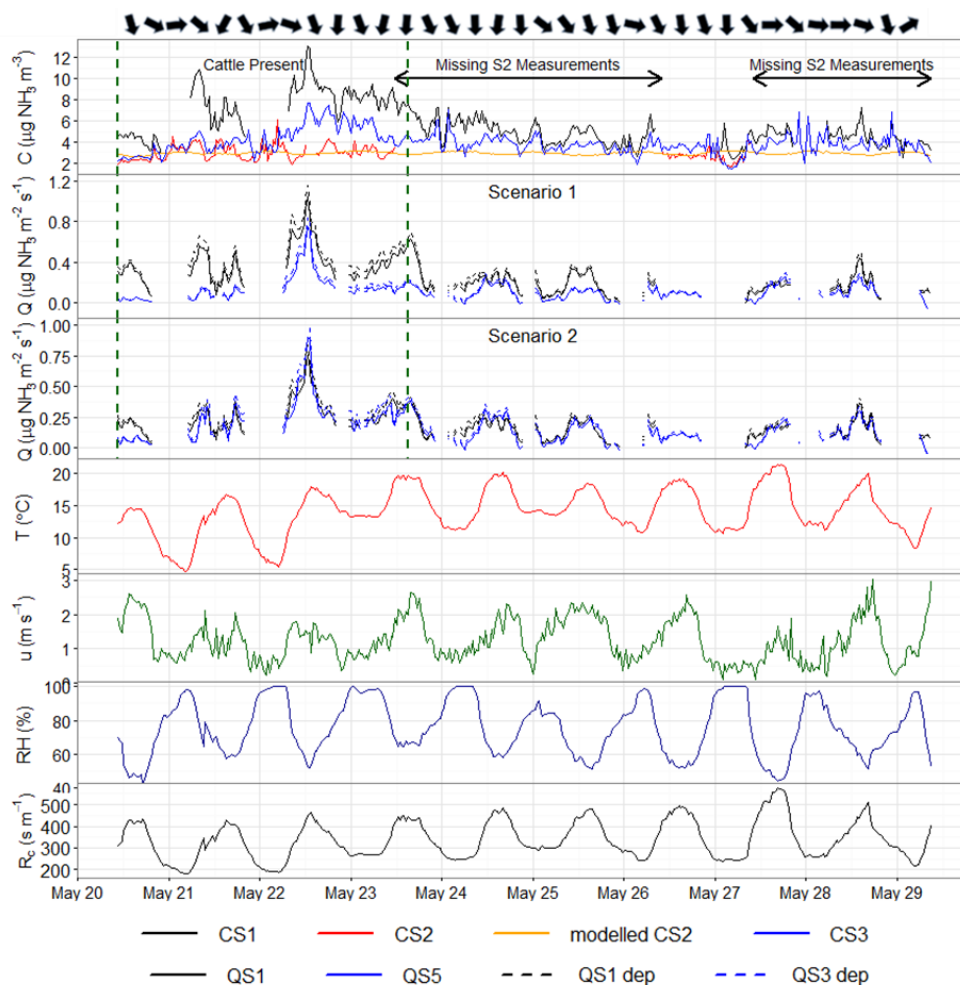
Figure 6: Timeseries of Period 2 DOAS concentration measurements (top panel) and bLS-R emission estimates (second and third panels, showing the Q (solid lines) and Q_{dep} (dashed lines) scenarios); with T, u, RH, and R_c (with 130 s m^{-1} offset) shown in the panels below. The second panel shows the Scenario 1 (homogenous field) emission estimates, while the third panel contains the optimised Scenario 2 estimates using the heterogeneous source area coefficients given in Table 1. Periods with missing S2 background concentration measurements are annotated on the top panel to highlight the higher uncertainty of these periods for emission estimates. Wind direction arrows are set above the top panel to visualise changes over time. The dashed green lines on the top panels mark the 3-day time period where the cattle were grazing the field.

832